CHAPTER 53

A MODEL TO PROPAGATE NONLINEAR WATER WAVES

J. M. Chambel Leitão*

J, L. M. Fernandes**

<u>Abstract</u>

The aim of the work presented here is to propagate random waves from deep or intermediate water depth to the nearshore region with a Boundary Integral Equation Method (BIEM) which is able to handle the nonlinear effects that occur in the process. A two-dimensional (x,z) mild nonlinear model to propagate waves over an uneven bottom is presented here. It takes into account 2nd order nonlinear effects of the wave transformation entering into shallow water. If energy dissipation is neglected, the flow field generated by the wave propagation can be described by a velocity potential formulation which is governed by the Laplace's equation in the domain. The results obtained from the model are time-dependent. The model is tested with solitary and irregular waves and compared with analytical and experimental results.

Introduction

The previous work done by the authors, (Fernandes, 1988) and (Leitão and Fernandes, 1989), led to the evidence that the computer CPU time required by a linear BIEM model (which cannot handle nonlinear effects) was relatively small whereas the nonlinear one was prohibitively expensive for real problems. This high cost is primarily due to the moving free surface boundary because the operation count includes forming a new coefficient matrix and solving the system every time step.

^{*} PhD student ** Assistant Professor Instituto Superior Técnico, Dep. Mechanical Engineering

Av. Rovisco Pais, 1096 LISBOA, PORTUGAL

A mild nonlinear model, was developed to meet the needs of afordable computer time and significant nonlinear effects. A Stokes-like expansion provided second order terms of the kinematic and the dynamic free surface boundary conditions that were introduced into a BIEM model. The important advantage of this is that these free-surface conditions are now applied at the mean water level which precludes moving elements. A constant coefficient matrix is used in this case. The boundary is discretized into linear elements and the time stepping is based on multistep integrators.

Basic Equations

Considering the flow to be irrotational and inviscid and the fluid to be incompressible, the Laplace's equation for the velocity potential (ϕ) is valid.

$$\nabla^2 \phi = 0 \tag{1}$$

This equation is subjected to a number of boundary conditions, namely: a) prescribed velocity (at the bottom or vertical boundaries),

$$\frac{\partial \phi}{\partial n} = \gamma(\mathbf{x}, \mathbf{z}, \mathbf{t}), \qquad (2)$$

where n is the unit outward normal; b) radiation (at vertical boundaries),

$$\frac{\partial \phi}{\partial t} + c \frac{\partial \phi}{\partial n} = 0, \qquad (3)$$

where c is the outgoing wave celerity; c) two nonlinear conditions (dynamic and kinematic) for the free-surface:

$$\frac{\partial \phi}{\partial t} + \frac{1}{2} |\nabla \phi|^2 + g\eta = 0; \qquad z = \eta \qquad (4)$$

$$\frac{\partial \eta}{\partial t} + \frac{\partial \phi}{\partial x} \frac{\partial \eta}{\partial x} - \frac{\partial \phi}{\partial z} = 0; \qquad z = \eta \qquad (5)$$

where η is the surface elevation.

690

2nd order free surface equations

In order to avoid problems and costs caused by a moving boundary on the numerical model, a Taylor series expansion of both dynamic and kinematic conditions is made about the level z=0.

$$\phi(\mathbf{x},\eta,t) = \phi(\mathbf{x},0,t) + \eta \frac{\partial \phi(\mathbf{x},0,t)}{\partial z} + \eta^2 \frac{\partial^2 \phi(\mathbf{x},0,t)}{\partial z^2} + O(\eta^3)$$
(6)

The following expressions result for the free-surface conditions, considering only the two first terms of the Taylor series:

$$\frac{\partial \Phi}{\partial t} + \eta \frac{\partial^2 \Phi}{\partial z \partial t} + g\eta + \frac{1}{2} \left(\frac{\partial \Phi}{\partial x} \right)^2 + \eta \frac{\partial \Phi}{\partial x} \frac{\partial^2 \Phi}{\partial z \partial z} + \frac{1}{2} \left(\frac{\partial \Phi}{\partial z} \right)^2 + \eta \frac{\partial \Phi}{\partial z} \frac{\partial^2 \Phi}{\partial z^2} = 0; \quad z = 0 \quad (7)$$

$$\frac{\partial \eta}{\partial t} + \frac{\partial \phi}{\partial x}\frac{\partial \eta}{\partial x} + \eta \frac{\partial^2 \phi}{\partial x \partial z}\frac{\partial \eta}{\partial x} - \frac{\partial \phi}{\partial z} - \eta \frac{\partial^2 \phi}{\partial z^2} = 0; \quad z = 0$$
(8)

In order to assess the importance of each term, dimensionless variables are introduced as follows:

$$\phi = \frac{AL}{T} \phi' ; \quad x = Lx' ; \quad z = h z' ; \quad t = Tt' ; \quad \eta = A\eta'$$

The typical scales used are: A - wave amplitude; L - wave length; T - wave period; h - depth. Using also parameters $\varepsilon = A/h$ and $\delta = h/L$ (dropping primes) expressions (7) and (8) result in:

$$\frac{\partial \phi}{\partial t} + \epsilon \eta \ \frac{\partial^2 \phi}{\partial z \partial t} + \frac{T^2}{L} \ g \eta + \epsilon \delta \ \frac{1}{2} \left(\frac{\partial \phi}{\partial x} \right)^2 + \epsilon^2 \delta \eta \ \frac{\partial \phi}{\partial x} \ \frac{\partial^2 \phi}{\partial x \partial z} + \frac{\epsilon}{\delta} \ \frac{1}{2} \ \left(\frac{\partial \phi}{\partial z} \right)^2 + \frac{\epsilon^2}{\delta} \eta \ \frac{\partial \phi}{\partial z} \ \frac{\partial^2 \phi}{\partial z^2} = 0$$
(9)

$$\frac{\partial \eta}{\partial t} + \epsilon \delta \frac{\partial \phi}{\partial x} \frac{\partial \eta}{\partial x} + \epsilon^2 \delta \eta \frac{\partial^2 \phi}{\partial x \partial z} \frac{\partial \eta}{\partial x} - \frac{1}{\delta} \frac{\partial \phi}{\partial z} - \frac{\epsilon}{\delta} \eta \frac{\partial^2 \phi}{\partial z^2} = 0$$
(10)

Neglecting terms of $O(\epsilon^2)$, $O(\epsilon^2/\delta)$ or larger and getting back to dimensional form, the free-surface conditions read:

- Dynamic
$$\frac{\partial \phi}{\partial t} = -g\eta - \frac{1}{2} |\nabla \phi|^2 - \eta \frac{\partial^2 \phi}{\partial z \partial t}$$
 (11)

- Kinematic
$$\frac{\partial \eta}{\partial t} = \frac{\partial \phi}{\partial z} - \frac{\partial \phi}{\partial x} \frac{\partial \eta}{\partial x} + \eta \frac{\partial^2 \phi}{\partial z^2}$$
 (12)

These equations are both valid at level z = 0 which allows the upper boundary in the numerical model to be constant in time. The last two terms of (11) and (12) account for the most important nonlinear effects while the others represent the linear ones.

Boundary Integral Element Method

The Laplace's equation with prescribed Dirichlet, Neumann, Robin and mixed boundary conditions is an elliptic problem which can be suitably solved by the BIEM. Our problem for the velocity potential is an hyperbolic one which includes variable time. Thus, we can use that method for the spatial discretization and let the time dependency be handled by a finite difference stepping scheme. A direct boundary element formulation, based upon Green's second identity, relates potential and normal velocity at the boundary. This way, the discretization involves only the boundary. For each element, x, z, ϕ , $\partial \phi/\partial n$ and η are piecewise linearly interpolated using their nodal values. Boundary conditions and unknowns can then be manipulated to form a system of equations. Having done this, one obtains an approximate solution that is equally accurate on both potential and normal velocity. The computation, upon request, of the potential and the velocity vector at interior points is explicit.

Time Marching Procedure

The free-surface equations for the second order model include linear terms, which are integrated by a trapezoidal rule (implicit), plus second order terms for which Adams predictorcorrector formulas are adequate. The blended predictor formulae are as follows:

Dynamic

$$\frac{1}{\Delta t} (\phi^{i+1} - \phi^{i}) = -\frac{g}{2} (\eta^{i+1} + \eta^{i}) + D_{P}^{(i,i-1)}$$
(13)

Kinematic
$$\frac{1}{\Delta t} (\eta^{i+1} - \eta^i) = \frac{1}{2} (\phi_z^{i+1} + \phi_z^i) + K_P^{(i,i-1)}$$
 (14)

Here D_p and K_p represent differences from linear equations and can be predicted as:

$$D_{P}^{(i,i-1)} = \frac{1}{4} \left(\phi_{x}^{2} + \phi_{z}^{2} \right)^{i-1} - \frac{3}{4} \left(\phi_{x}^{2} + \phi_{z}^{2} \right)^{i} + \frac{1}{2} \left(\eta^{i-1} \phi_{zt}^{i-1} - 3 \eta^{i} \phi_{zt}^{i} \right)$$
$$K_{P}^{(i,i-1)} = \frac{1}{2} \left(-3\phi_{x}^{i} \eta_{x}^{i} + \phi_{x}^{i-1} \eta_{x}^{i-1} - 3\phi_{x}^{i} \eta_{x}^{i} + \phi_{xx}^{i-1} \eta_{x}^{i-1} \right).$$

The corrector step makes use of the formulas:

Dynamic
$$\frac{1}{\Delta t} (\phi^{i+1} - \phi^i) = -\frac{g}{2} (\eta^{i+1} + \eta^i) + D_C^{(i+1,i)}$$
 (15)

Kinematic
$$\frac{1}{\Delta t} (\eta^{i+1} - \eta^i) = \frac{1}{2} (\phi_z^{i+1} + \phi_z^i) + K_C^{(i+1,i)}$$
 (16)

where D_{C} and K_{C} are given by: $D_{C}^{(i+1,i)} = -\frac{1}{4} \left(\phi_{x}^{2} + \phi_{z}^{2} \right)^{i+1} - \frac{1}{4} \left(\phi_{x}^{2} + \phi_{z}^{2} \right)^{i} - \frac{1}{2} \left(\eta^{i+1} \phi_{zt}^{i+1} + \eta^{i} \phi_{zt}^{i} \right)$ $K_{C}^{(i+1,i)} = -\frac{1}{2} \left(\phi_{x}^{i+1} \eta_{x}^{i+1} + \phi_{x}^{i} \eta_{x}^{i} + \phi_{xx}^{i+1} \eta^{i+1} + \phi_{xx}^{i} \eta^{i} \right).$

The numerical computation of the derivatives is omitted for brevity, beeing the vertical acceleration (ϕ_{zt}) the most unstable. A linear relation between ϕ and $\partial \phi / \partial n$ is sought with these formulae and it is accomplished by substitution of η^{i+1} in (13) with the corresponding expression taken from (14). The same is done for the correction procedure. Due to their linearity, other boundary conditions are of straightforward discretization in time.

Test Case 1

This first example aims to test the model with solitary waves propagating over a constant depth channel. Amplitudes were made to vary from 0.1 to 0.4 times the depth. From figure 1 an amplitude decay can be observed near the generation region and becoming less apparent as the wave moves rightwards. For

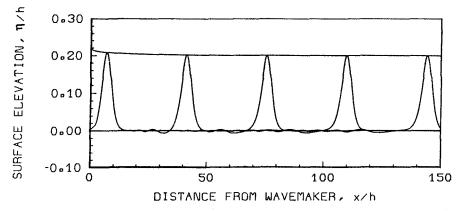


Figure 1. water surface profiles, for several time instants, and maximum amplitude curve along the channel; BIEM numerical results

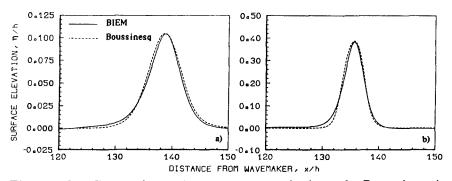


Figure 2. Comparison between numerical and Boussinesq's solitary wave profiles: a) $A/h \approx 0.1$; b) $A/h \approx 0.4$

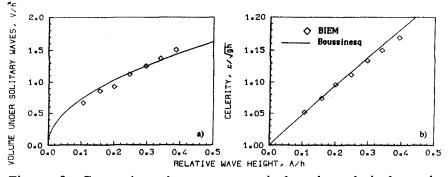


Figure 3. Comparison between numerical and analytical results for: a) volume under solitary waves; b) celerity

higher amplitudes this decay is more pronounced. Also a dispersive tail can be seen as the wave propagates. In figures 2a and 2b comparisons are made between the numerical profiles and the analytical solution of Boussinesq. These numerical profiles where taken when the wave reached the right end of the channel and had already an almost constant amplitude. The agreement seems good. Computations of celerity and of the volume under the solitary waves are also compared with their corresponding analytical values available from Boussinesq's theory (figure 3). Again both numerical and analytical values agree well and even the different trend that can be identified in the numerical results of celerity is also present on some experimental results (Goring, 1978). The CPU time needed for each run (1000 time steps and 620 nodes) was about 6m30s on a CONVEX C220.

Test Case 2

A solitary wave propagating over a step is tested and results are compared with experiments by (Goring, 1978). In figure 4 time series of surface elevation at several points are displayed along with some experimental values. The effects of viscosity and bottom and wall shear, present when a real wave propagates on a channel, tend to decrease the amplitude of the wave. Since those effects are not accounted for on the numerical model, differences found both in amplitude and phase should be expected. The second wave on gauge 1 is the one reflected from the step which, after reflecting again on the generation plate, appears once more on that same gauge. This second reflection on the generator is not present on the experimental results maybe because that wavemaker had a nonreflecting surface. After passing over the step, the solitary wave evolves into three solitary waves. On gauge 5 those three waves, going to and coming from the right wall, can be very distinctly observed. Figure 5 shows the free-surface numerical profile when the first and second waves are almost completely formed. They are compared with two analytical Boussinesq's profiles of equal amplitudes. The CPU time needed for this example (3500 time steps and 683 nodes) was 22 min on a CONVEX C 220.

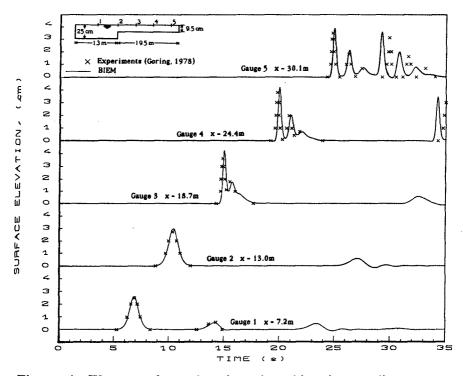


Figure 4. Water surface elevation time histories at five gauges along the channel; comparison between BIEM and experimental results

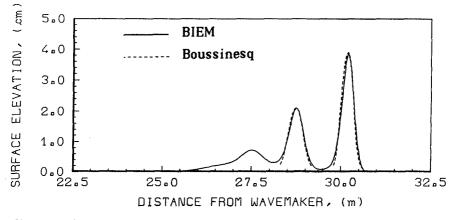


Figure 5. BIEM water surface profile; comparison with Boussinesq's theoretical solitary wave profiles

Test Case 3

The shoaling of random waves is a problem of current interest and it is addressed here in the perspective of comparing experimental and field results with numerical BIEM results. A limitation of this numerical model is that it cannot include breaking effects on shoaling studies. As this is a second order model, propagating waves of two individual frequencies, say f_i and f_j , would produce waves of frequency f_i+f_j and f_i-f_j . For a continuous spectrum, energy is tranferred to lower and higher harmonics of the peak frequency; see for example (Mansard et al.,1988).

Three random wave cases were simulated with three different significant wave heights (5.0, 8.0 and 8.5 cm) each corresponding to a Bretschneider spectrum with 0.6 Hz peak frequency. The effects of shoaling, on a 1/20 slope, upon spectral shape, groupiness factor, shape factor of Weibull Distribution and skewness of water surface variation are investigated and compared, when it was possible, with experiments from (Mase, 1989). Although Mase's experiments were made by taking several samples from a spectrum (Pierson-Moskowitz with peak frequency of 0.6 Hz) but with different groupiness factors, the 3 numerically generated samples of random waves used in this study had 3 different spectra for each one and no imposed groupiness factor.

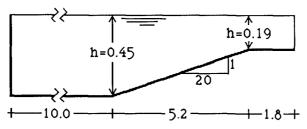
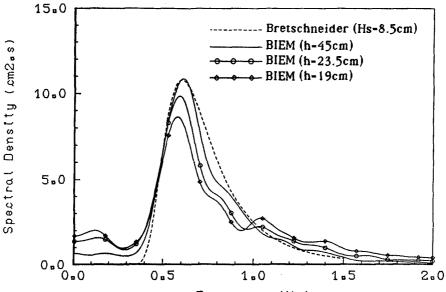


Figure 6. Numerical flume (dimensions in meters)

The "numerical flume" in figure 6, had the generation region at 45cm depth, and a slope of 1/20 until 19 cm depth. At the right end of the channel a radiation boundary is used. The referred experiments of (Mase, 1989) also include the breaking region. Records of surface elevation were stored for 50 nodes of the free-surface during 250 sec., containing about 170 waves, and for each one a time and frequency analysis was done. The spectra in fig. 7 are: the one imposed, with a significant wave height of 8.5 cm and source of the random wave sample, and the other three result from the frequency analysis at 45cm (toe of the slope), 23.5cm and 19 cm depth. Sub and superharmonics appear very clearly for decreasing depths in fig. 7. This energy transfer inside the spectrum, a nonlinear effect, is present when waves reach shallow water.



Frequency (Hz)

Figure 7. Spectra resulting from numerical BIEM data frequency analysis at several depths and source spectrum of the random waves introduced at the left end of the channel

The most important parameters computed were:

- The groupiness factor (GF) calculated from SIWEH (Funke and Mansard, 1979);

- The shape factor of the one parameter Weibull Distribution (m) (Cohen, 1965);

- The skewness of water surface variation ($\sqrt{\beta_1}$);

- The spectral width parameter Qp defined by (Goda, 1970).

In fig. 8 the variation of Qp along the slope can be seen and, though no comparison is made with other results, the trend seams to be correct according to data from (Thompson and Vincent, 1985). In fig. 9 the variation of the groupiness factor and the skewness along the slope is shown. When compared with results from (Mase, 1989) it can be seen that for similar tests similar values and trends are encountered. A correlation between the groupiness factor and the shape factor of Weibull Distribution proposed by (Mase, 1989) is presented in fig. 10 with some of the numerical results. These seem to fit quite well in the 95% confidence interval.

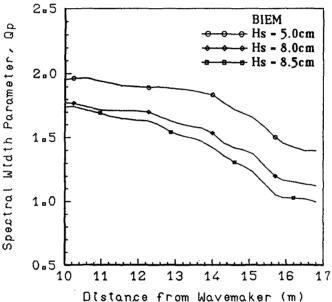


Figure 8. Spectral Width Parameter along the 1/20 slope

Conclusions

A 2nd order BIEM model to propagate waves in intermediate and shallow water was presented. The tests made with solitary and irregular waves showed that it can handle quite well nonlinear waves up to, at least, 0.4 of relative wave height. Although it cannot include breaking effects, studies of irregular wave propagation are possible within a moderate range of relative wave heights (this limit would be about $0.5 \text{Hm}_0/\text{h}$

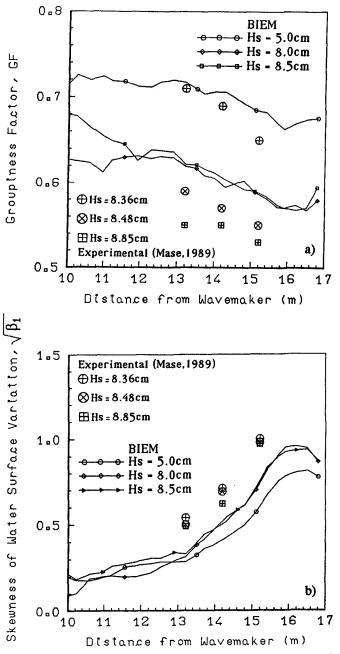


Figure 9. Variation along the 1/20 slope of: a) the Groupiness Factor; b) the Skewness of Water Surface Variation

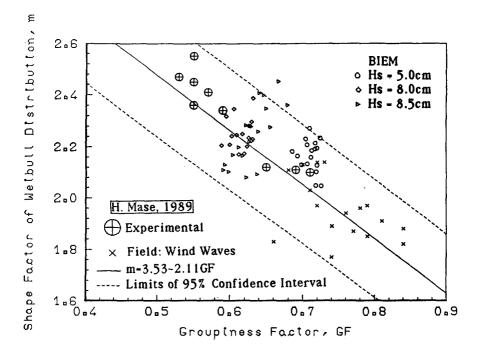


Figure 10. Relationship between Groupiness Factor and Shape Factor of Weibull Distribution

although it was not thoroughly studied). In that range of relative wave heights it is possible to compute pressure inside the 2D domain which allows also to evaluate forces acting on submerged bodies. Depending on the size of the discretization, this model is about 10 times faster than a fully nonlinear BIEM model. The ideas presented here can be extended to three-dimensional problems as more computer power becomes available.

Acknowledgements

This work and the first author are supported by Junta Nacional de Investigação Científica e Tecnológica under contract n° 87472.

References

Cohen, A. C., "Maximum likelihood estimation in the Weibull Distribution based on complete and on censored samples", Technometrics, Vol.7, No. 4, November 1965.

Fernandes, J.L.M., "A boundary element method for nonlinear water waves", Proc. Computer Modelling in Ocean Engng, Eds B. A. Schrefler & O. C. Zienkiewicz, Balkema, September 1988.

Funke, E.R., Mansard, E.P.D., "On the synthesis of realistic sea states in a laboratory plume", Hydraulics Laboratory, Report n° LTR-HY-66, National Research Council of Canada, Ottawa, Canada, August 1979.

Goda, Y., "Numerical experiments on wave statistics with spectral simulation", Report of the Port and Harbour Research Institute, 9(3), 1970.

Goring, D.G. "Tsunamis - The propagation of long waves into a shelf", W.M. Kech Laboratory of Hydraulics and Water Resources, Report n^o KH-R-38, California Institute of Technology, Pasadena, California, November 1978.

Leitão, J.M.C. and Fernandes, J.L.M., "Numerical solution of linear wave propagation problems", Proc. 4º Simpósio Luso-Brasileiro de Hidráulica e Recursos Hídricos, Ed. APRH, Lisboa (in Portuguese), June 1989.

Mansard, E. P. D., Sand, S. E., Klinting, P., "Sub and Superharmonics in natural waves", Journal of Offshore Mechanics and Arctic Engineering, Vol. 110, August 1988.

Mase, H., "Groupiness factor and wave height distribution", Journal of Waterway, Port, Coastal and Ocean Engineering, Vol. 115 n° 1, January 1989.

Thompson, E.F., Vincent, C.L. "Significant wave height for shallow water design", Journal of Waterway, Port, Coastal and Ocean Engineering, Vol. 111, n° 5, September 1985.